Contextually-aware Fetal Sensing in Transabdominal Fetal Pulse Oximetry

Abstract—Transabdominal fetal pulse oximetry (TFO) is a noninvasive technique that can provide physicians with a convenient measure of fetal oxygen saturation. This is accomplished by sending a known light intensity signal towards the mother's abdomen, where it is modified by the maternal and fetal tissues, and observed some distance away. The measured signal, captured by a photodetector, contains a mixture of both maternal and fetal information, where the fetal portion must be extracted to calculate the fetal oxygen saturation. However, the ability to decouple the maternal and fetal components is highly dependent on the physiological and structural parameters of the physical system. In this work, we propose a contextually-aware sensing approach that utilizes additional information about the physical system (physiological, spatial, and temporal) to extract the fetal signal. It does this by using easily-measurable parameters of the mother's physiology to reduce the maternal impact, incorporating data fusion techniques to combine spatial information from multiple detectors, and utilizing historical data points to improve and validate the fetal signal estimates. The efficacy of the proposed approach is supported by experimental evaluation using in vivo measurements captured on pregnant sheep.

I. INTRODUCTION

Currently, physicians use cardiotocography (CTG) to monitor fetal well-being during active labor. This technique evaluates the temporal relationship between uterine contractions and changes in the fetal heart rate to identify signs of distress. It is thought that decelerations in the fetal heart rate after a uterine contraction is a sign of fetal distress. If occurring over a long duration, it can be an appealing option to perform an operative intervention (i.e. C-section) to quickly remove the child. However, since its introduction, CTG has been shown to have a horrendously high false-positive rate (99.8% for cerebral palsy [1]), which has partly led to a significant rise in emergency C-sections without reducing the rates of adverse fetal outcomes [2]. C-sections are major abdominal surgeries, which increase costs and health risks to both the mother and child, such as higher-rates of type-1 diabetes, chronic lung conditions, and post-operative complications [3]-[5]. Currently, 1 in 3 children are born via C-section in the United States [6] which exceeds the recommended range (10-15%) put forth by the World Health Organization [7], [8]. In addition to a mediocre interpretation reliability amongst obstetricians [9], a large proportion of C-sections are performed in response to a non-reassuring CTG trace [10], making it clear that this high-cost (increased C-sections) and low-benefit (no change in adverse fetal outcomes) monitoring scheme needs

Transabdominal fetal pulse oximetry (TFO) can potentially improve fetal outcomes by providing physicians with a more

objective metric of fetal well-being, namely fetal oxygen saturation. This technique uses light to investigate the underlying fetal tissue through a reflectance-based optical probe placed on the maternal abdomen. Variations in the diffused light intensity signal are caused by physiological changes in tissue composition, and can be analyzed to estimate the fetal oxygen saturation. A high-level diagram of transabdominal fetal pulse oximetry (TFO) can be seen in Figure 1.

In general, light-based measurement modalities operate by sending a known light signal into the body, where it is modified by the human tissue, and observed some distance away. In TFO, both maternal and fetal physiology causes the tissue composition to change, resulting in a mixed (maternal+fetal) signal. Since photons must first travel through the mother's abdomen before reaching the fetus, any photons containing fetal information will be corrupted with maternal noise. In addition, the number of photons that reach the fetus is highly dependent on the fetal depth, which varies between patients and as natural birth progresses. These structural and physiological dynamics makes extracting the fetal signal challenging.

To address the fetal signal extraction problem, we propose a contextually-aware approach that extracts the fetal signal by incorporating additional information about the physical system (physiological, spatial, and temporal). It does this by utilizing knowledge about the mother's physiology to reduce the maternal noise (physiological), incorporating spatial-information from multiple detectors to increase robustness to unknown changes in fetal depth (spatial), and utilizing historical measures of the fetal signal to improve and validate new estimates of the fetal signal (temporal). This represents a tightly-coupled cyber-physical system where the proposed contextually-aware approach incorporates knowledge of the physical system to process the raw measurements in the cyber-system, and expose an underlying physical signal (fetal signal). To accomplish this, we perform the following:

- First, we characterize the physical system by decomposing the mixed signal into its constituent parts and performing Monte Carlo simulations, to profile the relationship between the mixed signal the physiological and spatial parameters.
- Afterwards, we present the proposed contextually-aware fetal sensing approach, which incorporates information about the physical system, to extract the fetal signal, and describe the details of each submodule.
- Lastly, we evaluate the proposed approach using in vivo measurements captured on pregnant sheep/hypoxic fetal lambs, using our transabdominal fetal oximetry system.

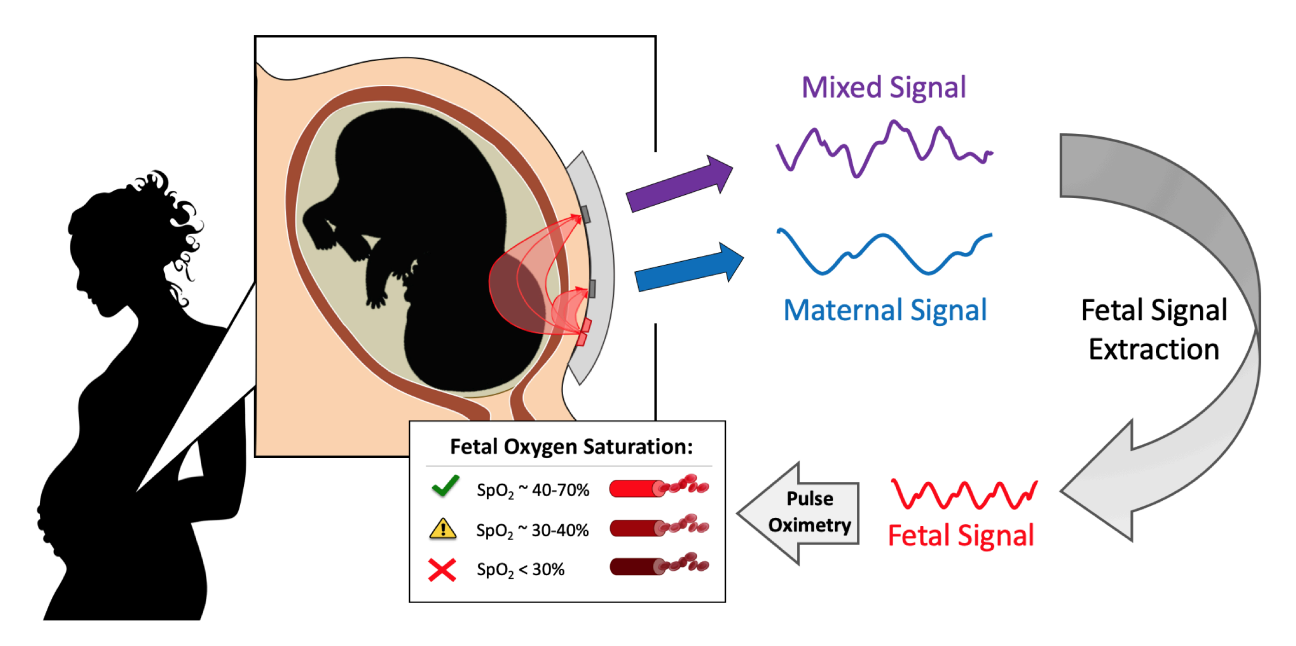


Fig. 1. A high-level overview of Transabdominal Fetal Pulse Oximetry [11]. Photons are sent through the maternal abdomen to investigate the fetal tissue, before propagating back to a photodetector on the optical probe (optode) as a mixed (maternal+fetal) signal. Fetal signal extraction is performed to decouple the maternal and fetal signals, before estimating the fetal oxygen saturation through conventional pulse oximetry calculations.

II. BACKGROUND

A. Overview of Pulse Oximetry

Pulse oximetry is a non-invasive method to estimate the relative concentration of oxygenated hemoglobin in arterial blood. At its core, it uses the Beer-Lambert Law, which describes the changes in light intensity with respect to the concentration of chromophores in a medium and the relative distance between the light source and detector:

$$I_t(\lambda) = I_0(\lambda) * 10^{-\sum_i c_i(t) * \epsilon_i(\lambda) * L}$$
 (1)

where I_t is the measured light intensity at a detector at time t of wavelength λ , I_0 is the incident light intensity, c_i and ϵ_i is the concentration and molar extinction coefficient of the i^{th} chromophore in the medium, and L is the path-length a photon takes to get to the detector from the light source. This can be written in terms of the relative change in absorption (ΔA) between times t1 and t2 in the Modified Beer-Lambert Law (MBLL):

$$\Delta A = -\log_{10}(I_{t2}(\lambda)/I_{t1}(\lambda)) = \sum \Delta c_i * \epsilon_i * \langle L \rangle$$
 (2)

The expected photon path-length $(\langle L \rangle)$ is used here since discontinuities in the refractive index in a medium can cause photons to non-deterministically scatter from their initial trajectory.

When the medium is human tissue, cardiac contractions cause arterial vascular tissue to pulsate accordingly. This results in small, periodic dips in light-intensity seen at a detector, also known as a photoplethysmogram (PPG), and allows the optical capture of a person's heart rate. In addition, since oxy- and deoxy- hemoglobin (HbO2 and Hb) absorb light at different levels in the red and near-infrared (NIR)

spectral regions, analyzing the depth of light attenuation (ΔA) from PPGs captured at these wavelengths can be used to infer the arterial blood-oxygen saturation (SpO2).

$$SpO2 = c_{HbO2}/(c_{HbO2} + c_{Hb})$$
 (3)

In pulse oximetry, SpO2 is proportional to a modulation ratio (R) which is defined as the ratio of two PPGs taken in the red $(\lambda 1)$ and NIR $(\lambda 2)$ wavelengths.

$$R = \frac{\Delta A_{\lambda 1}}{\Delta A_{\lambda 2}} = \frac{\log_{10}(I_{systole,\lambda 1}/I_{diastole,\lambda 1})}{\log_{10}(I_{systole,\lambda 2}/I_{diastole,\lambda 2})} \propto SpO2 \quad (4)$$

This proportionality factor is empirically determined using a large number of healthy volunteers through the gold-standard invasive blood-gas analysis measurements during controlled desaturation experiments.

B. Transabdominal Fetal Pulse Oximetry

Transabdominal fetal pulse oximetry (TFO) is a fully non-invasive technique to measure fetal oxygen saturation. This is accomplished by sending photons through the maternal abdomen to investigate the underlying fetal tissue using a reflectance-based optical probe (optode). The photons propagate through the maternal and fetal tissues, which causes the light intensity (signal) to vary according to the Beer-Lambert Law. Some of the photons that reach the fetus diffuse back towards the skin surface and are captured by a photodetector, where the resulting mixed (maternal+fetal) signal is measured, processed, and analyzed to extract the fetal signal, which is used to estimate fetal oxygen saturation through conventional pulse oximetry calculations. A highlevel view of this technique can be seen in Figure 1.

1) Mixed Signal Problem: In TFO, photons that contain fetal information must make a round-trip through the mother's abdominal wall before reaching a detector. However, physiological processes causes temporal changes in the mother's tissue composition, which alters the signal. Expanding the MBLL for both maternal and fetal tissues, the signal measured at a detector can be written as:

$$\Delta A = \frac{1}{\ln(10)} (\Delta \mu_{a,mat} * \langle L_{mat} \rangle + \Delta \mu_{a,fet} * \langle L_{fet} \rangle) + \xi$$
 (5)

where ΔA is the measured change in absorptivity at a detector, $\Delta \mu_{a,mat}$ and $\Delta \mu_{a,fet}$ are the changes in absorption coefficients caused by maternal and fetal tissues respectively, $\langle L_{mat} \rangle$ and $\langle L_{fet} \rangle$ are the expected partial path-lengths photons take to reach the detector through respective tissues, and ξ represents other noise factors seen in the measurement (e.g. thermal noise) caused by the physical components used and is considered to be Gaussian-distributed with zero-mean. Note that we use the absorption coefficient (μ_a) here instead of the molar extinction coefficient (ϵ) . Both provide a measure of light attenuation and are related by $\mu_a = \ln(10) * \epsilon * c$.

In order to estimate the fetal oxygenation using Equation 4, the fetal signal must be extracted from the mixed signal. Given the stochastic nature of light scattering and absorption, decoupling the maternal and fetal signals can be challenging. One approach is to use a conventional pulse oximeter on the mother's finger, to estimate the maternal contribution and remove it from the mixed signal. This helps to provide an additional measure of the mother's cardiac response, but may not fully represent the signal seen at the maternal abdomen, where respiration effects are more evident. Further measures of the mother's physiology may be helpful in fully removing the maternal contribution from the mixed signal.

2) Fetal Depth Variations: Prior to birth, the fetus resides in the uterus and is typically located several centimeters within the maternal abdomen. For highly-scattering materials like tissue, this is optically deep, meaning that only a small proportion of photons reaching a detector will have traversed fetal tissues. In general, signals seen at the skin surface are more sensitive to changes in the superficial (i.e. maternal) tissues, and thus, the maternal noise dominates the mixed signal.

For reflectance-mode sensors, the relative distance between the light source and photodetector (source-to-detector or SD distance) plays an important role in increasing the depth of tissue investigated. The larger the SD distance, the deeper the tissue being investigated but at a cost of overall light intensity (strength). Optimizing this parameter can be difficult, since patient variability can cause the fetal depth to vary drastically. This can occur between different patients, or as the fetus moves through the birth canal during natural delivery, and causes the optimal SD distance to vary between patients and over time [11]. To design a clinically-robust TFO system, it is important that the fetal signal extraction must be robust to both *inter-* and *intra-* patient variability.

III. PROBLEM STATEMENT

As previously described, the mixed signal is a result of changes in tissue composition caused by maternal and fetal physiology. In addition, the signal's sensitivity to fetal tissues is highly dependent on anatomical parameters like fetal depth. Since tissue is a highly-scattering material, small changes in fetal depth can have significant effects on the ability to capture sufficient fetal information. To address this problem, we propose a contextually-aware approach that can extract the fetal signal by utilizing additional knowledge about the physical system, namely physiological, spatial, and temporal information. In this work, we first characterize the physical system by decomposing the mixed signal into its constituent parts, and simulate photon propagation through representative tissue models to profile the relationship between spatial parameters to the mixed signal. Next, we present the contextuallyaware approach and describe its various submodules in detail. Lastly, we evaluate the efficacy of the approach to identify the fetal signal, by developing a TFO system prototype and capturing in vivo measurements on pregnant sheep.

IV. CHARACTERIZING THE PHYSICAL SYSTEM

In this section, we characterize the physical system in order to understand its effect on the mixed signal. In particular, we decompose the mixed signal into maternal and fetal components and describe the physiological changes that cause the light intensity to vary, and simulate photon propagation through representative tissue models to profile the relationship between fetal depth, SD distance, and fetal signal sensitivity (i.e. the proportion of signal that contains fetal information).

A. Decomposing the Mixed Signal

To understand the relationship between the mixed signal and the underlying physiology it describes, we decompose the mixed signal into the maternal and fetal components and rewrite Equation 5 as:

$$\Delta A = \Delta A_{mat} + \Delta A_{fet} + \xi \tag{6}$$

where ΔA_{mat} and ΔA_{fet} are the changes in absorptivity due to maternal and fetal tissues respectively. In TFO, identifying ΔA_{fet} is the goal. These changes are caused by the slight arterial expansion from heart contractions occurring at the fetal heart rate (FHR), typically occurring between 2-5 Hz [12]. As described in Section II-B, this signal forms the basis upon which fetal oxygen saturation can be calculated.

Physiological changes in the maternal tissue ΔA_{mat} are also present in the mixed signal. Some of these changes are caused by the mother's respiration and cardiac cycles:

$$\Delta A_{mat} = \Delta A_{mat}^{Resp.} + \Delta A_{mat}^{Cardiac} \tag{7}$$

In the cardiac cycle, arterial vascular tissues expand slightly with each heart contraction, which increases the blood-tissue volume ratio. Depending on the tissue perfusion, the amount this rises typically varies between 2-10% [13]. While this is a small percentage, it is enough to create a PPG waveform that is used in conventional pulse oximetry. This maternal PPG

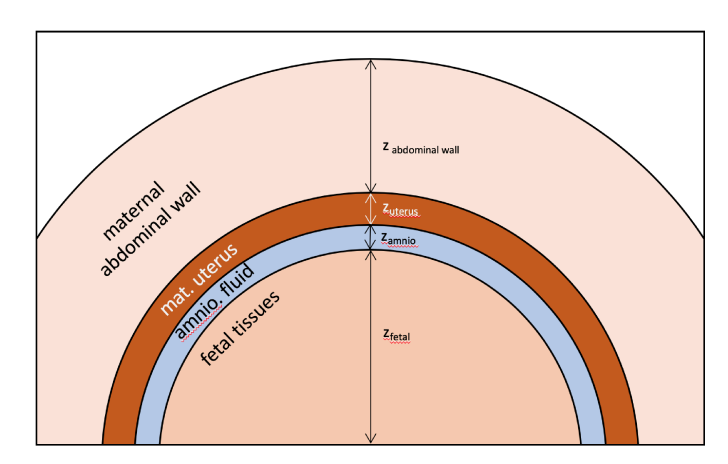


Fig. 2. Tissue Model used in the Monte Carlo simulations. It consists of four spherical regions, representing the maternal abdominal wall, maternal uterus, amniotic fluid, and fetal tissues. Their physical dimensions and optical properties can be seen in Table I.

waveform is synchronous with the maternal heart rate (MHR) which typically occurs between 1-2 Hz. A number of common medical devices can be used to measure the MHR, including electrocardiogram (ECG) and conventional pulse oximeters.

Similarly, artifacts caused by respiration (breathing) may also be present in ΔA_{mat} . These respiratory induced variations (RIV) are thought to be caused by changes in the peripheral venous pressure and increased rate of venous return [14]–[16]. While the variations change synchronously with respiration rate (RR), its intensity is highly variable, pending ventilation and physical parameters like tidal volume, body position, and probe location [14]. Typically, respiration occurs between 0.1-0.5 Hz. Respiratory rate can be monitored through non-invasive nasal capnography.

B. Maternal-Fetal Contribution via Monte Carlo Simulations

While physiological changes in both maternal and fetal tissues can cause the light intensity to change, their relative contribution to the mixed signal can vary depending on which tissues the photons traversed. Several key parameters that affect this are the optical and physical properties of the tissues. Importantly, the SD separation and fetal depth play a significant role in the ability to capture sufficient fetal information. To characterize this relationship, we simulated photon propagation through representative tissue models, and measured the fetal signal sensitivity, defined as the proportion of photons that traversed the fetal tissue to total photons seen at a detector.

1) Tissue Models: To model light propagation in the intrapartum environment, we developed volumetric tissue models that consisted of four spherical tissue regions, representing the maternal abdominal wall, the uterus, amniotic fluid, and the fetus, and are illustrated in Figure 2. Their optical properties and physical dimensions were obtained through the literature, and can be seen in Table I. To evaluate different fetal depths, five tissue models were developed. Each tissue model had a different abdominal wall thickness, to establish fetal depths

TABLE I Optical Properties of Tissue Model

Tissue Type:	$\mu_a~(\mathrm{mm}^{-1})$	$\mu_s~(\mathrm{mm}^{-1})$	g (unitless)	n (unitless)	z (cm)	Ref.
Maternal Abdominal Wall	0.009	12.003	0.9	1.4	0.2 - 4.2	[18], [19]
Maternal Uterus	0.01	8.15	0.9	1.4	0.7	[20]
Amniotic Fluid	0.004	0.1	0.9	1.334	0.1	[21]
Fetal Tissues	0.013	9.916	0.9	1.4	10	[22], [23]

ranging from 1 to 5 cm, matching those seen in the patient population [17].

2) Monte Carlo Simulations: Given the stochastic nature of photon propagation through highly-scattering materials like tissue, numerical techniques like Monte Carlo simulations are often used. We utilized a well-verified, GPUaccelerated Monte Carlo simulation to evaluate photon propagation through each of the aforementioned tissue models [24]. In this approach, photons are injected into a tissue model, and its propagation through the tissue is monitored until it escapes at the tissue surface or extinguished by the tissue. A detailed description of the propagation algorithm can be found in Fang and Boas' work [24], and its salient points are summarized here. Photon propagation through the tissue is accomplished by using the optical properties of the tissue, which describes the absorption and scattering probabilities, the scattering anisotropy, and the index of refraction. At each step, a photon is moved through the tissue and its energy is decreased according to the Beer-Lambert Law, and a probability of scattering is determined using the optical properties to seed an exponentially-weighted probability function. If a scattering event occurs, the scattering direction is obtained through the Henyey-Greenstein scattering phase function while considering Fresnel's equations at the tissue boundaries, and the photon position and direction is updated. This process is repeated until all photons are either extinguished through absorption or escapes at the surface. Photons escaping at the surface that also hit a detector are recorded to analyze information about the tissues it traversed.

For each tissue model, 10 simulations were performed, where each simulated 160 million photons propagating through the tissue model at a wavelength of 850 nm. Detectors were placed on the maternal abdomen with SD distances at 1.5, 3, 4.5, 7, and 10 cm. Photons exiting the tissue that interact with these detectors were recorded, to provide context on the overall signal strength and the fetal signal sensitivity.

C. Results and Discussion

In total, 1.6 billion photons were simulated for each tissue model, which provided sufficient information for the sensitivity to converge at deeper fetal depths. Utilizing a GPU-accelerated Monte Carlo tool [24], it took ~8 hrs to complete all of the simulations, which is much faster than single-threaded approaches which would have taken several days [19]. The effect that SD distance and fetal depth have on the fetal signal sensitivity can be seen in Figure 3. As we can see, detectors with large SD distances capture a higher proportion of photons that reach the fetus than those with small SD distances. In particular, the fetal signal sensitivity

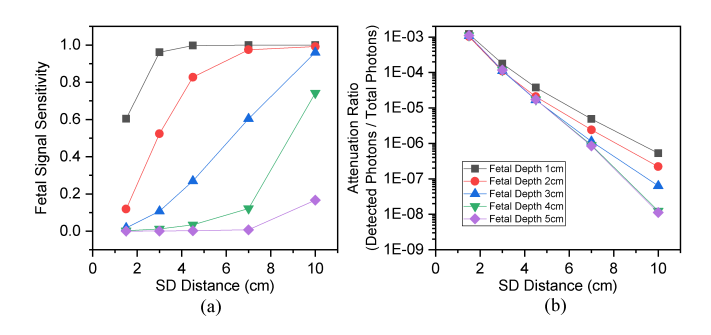


Fig. 3. Results from the Monte Carlo simulations. a) Fetal Signal Sensitivity (ratio of photons that traversed fetal tissues to total photons seen) at various SD separations and fetal depths, b) Attenuation ratio vs SD separation (ratio of number photons seen to total photons injected into the tissue).

monotonically-increases with SD distance, but decreases with fetal depth. This is expected, since it is harder for photons to reach the fetus when it is deeper. However, the attenuation ratio, defined as the number of detected photons over the total photons introduced into the skin, exponentially decreases with SD distance, as described in Equation 1. In practice, fetal depth is unavailable during the intrapartum period, and thus, it is difficult to determine if *sufficient* fetal information is being captured by a detector, without additional context.

V. CONTEXTUALLY-AWARE FETAL SENSING APPROACH

As argued previously, the structural and physiological dynamics of the physical system makes it difficult to decouple the fetal and maternal components from the mixed signal. In this section, we present a contextually-aware approach that extracts the fetal signal by incorporating additional information about the physical system (physiological, spatial, and temporal). In particular, we utilize external measures of the mother's physiology to reduce the maternal noise (physiological), incorporate known information about the SD distance to increase robustness to unknown fetal depths through data fusion techniques (spatial), and by utilizing historical estimates to improve the ability to track and validate the fetal signal (temporal). We assume that external measures of fetal information are unavailable, as existing methods may interfere with the TFO optode due to similar placement requirements on the mother. A high-level diagram of the proposed approach can be seen in Figure 4(b). In the following, each of the modules are described in detail.

A. Maternal Noise Reduction

In the proposed approach, we incorporate external measures of the mother's physiology to reduce the maternal noise seen in the mixed signal. As we described in Section IV-A, the source of maternal noise is caused by respiration and cardiac contractions. Therefore, we utilize the mother's respiration rate (MRR) and heart rate (MHR) to generate filters that reduce their contribution to the measurements. Given the periodicity of these physiological signals, we analyze the TFO measurements in the frequency domain. First, we generate the frequency-domain representation of each channel's raw

data using the fast-fourier transform and estimate their power spectral densities (PSD). The PSDs, in conjunction with external measures of the MRR and MHR, are used by the filter generator to create ideal notch filters centered at the MHR and MRR frequencies, and their associated harmonics identified as strong peaks in the PSD at integer multiples of the fundamental frequencies. Harmonics up to 6 Hz are considered, since the fetal signal should be present within 2-5 Hz. The signals are sent through the associated filters to reduce the maternal noise in each of the channels.

$$\Delta A_{filtered} = \Delta A_{fet} + \xi \tag{8}$$

After maternal noise reduction, the filtered signals should consist of only the fetal signal and random noise, as shown above.

B. Data Fusion

In addition to incorporating physiological information, we use data fusion to combine the measurements seen at each detector (channel) to improve the fetal signal estimation. After reducing the maternal noise, only the fetal content and random noise should remain in each of the channels. However, if the measurements are captured from a detector with a small SD separation, it may not contain sufficient fetal information (i.e. $\Delta A_{fet} \approx 0$), whereas channels with a larger SD distance will have higher fetal sensitivity but captures less photons overall. Importantly, the fetal sensitivity monotonically increases with SD distance. We use this information to combine the measurements from each channel using a weighted-sums approach where the weights represent the SD distance for respective detectors, and thus provides a measure of relative fetal information contained in that channel.

$$\Delta A_{wsums} = \sum_{i} w_i * \Delta A_{filt.,i} = \sum_{i} w_i * (\Delta A_{fet,i} + \xi_i)$$
 (9)

As seen in Figure 3, the shape of the fetal sensitivity to SD distance relationship changes with fetal depth. However, fetal depth is an unavailable parameter, and thus this knowledge cannot be utilized. For this reason, we define our weights as linear, evenly-separated weights between 0 and 1, where the weight for the largest SD distance is assigned the value of 1 and smaller SD distances closer to 0. This linear-weighting approach aims to improve robustness to unknown changes in fetal depth.

In addition to incorporating spatially-aware sensing through data fusion technique, another benefit is that the variance of ξ is reduced in the fused signal. Since ξ_i represents the random, Gaussian-distributed with zero-mean, noise seen in the i^{th} channel, the expectation of $\sum w_i * \xi_i$ will also be a Gaussian-distributed, zero-mean random variable with reduced variance, thus improving the fetal signal-to-noise ratio.

C. Fetal Signal Estimation

After data fusion, the resulting signal is then sent to the fetal signal estimation module. In a simple manner, this module uses the power spectral density of the fused signal, and searches

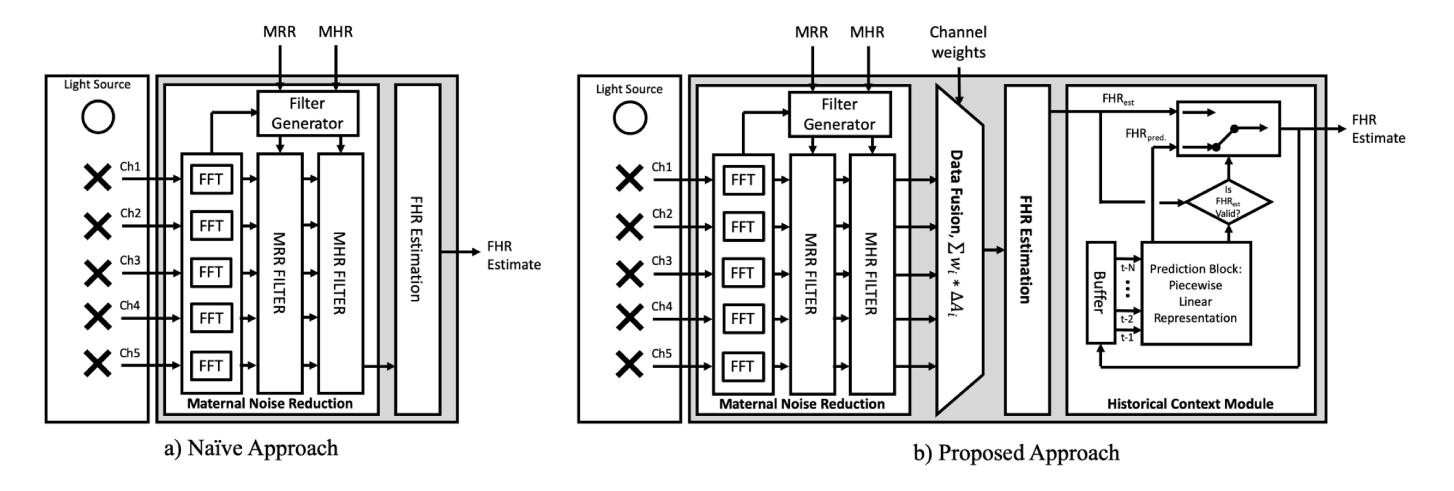


Fig. 4. A high-level view of the a) Naïve Method and b) Proposed Approach, which consists of a maternal noise reduction, data fusion, fetal heart rate estimation, and historical context submodules. These submodules incorporate additional information about the physical system, used to extract the fetal signal.

for the maximum power within lower- and upper- bounds of typical fetal heart rates. We define the FHR prior as having a lower bound of 2 Hz and an upper bound of 5 Hz, as characterized in the literature [12]. This simple approach is possible, because of the processing from earlier modules which reduced the maternal noise and incorporated spatial context into the fused signal.

D. Historical Context Module

As previously mentioned, physiological signals are non-stationary, in that the fetal and maternal signals can vary over time. In the case where the FHR moves behind the maternal components or one of their harmonics, the maternal noise reduction block will incorrectly filter away the fetal signal. This causes the simplistic fetal estimation method to incorrectly identify the fetal heart rate. To address this issue, we use previous fetal estimates to generate a prediction model, which is used to validate the fetal signal estimate based on its trajectory. In this manner, we improve the fetal estimates by utilizing temporal context into the approach.

Historical fetal estimates are used to generate a prediction model (piecewise-linear representation) used to predict the next fetal heart rate (FHR $_{pred.}$), and determine the validity of the estimated fetal heart rate (FHR $_{est}$). If the estimate is similar to the prediction, then FHR $_{est}$ is deemed valid and is passed through to the output. However, if they differ drastically, we consider the estimate to be *invalid*, and use FHR $_{pred.}$ as the result. For our system, we consider a valid change in FHR to occur within 0.35 Hz (or 21 bpm), which covers 97% of the variation seen in the clinic [25].

$$\label{eq:fhresult} \begin{aligned} \text{FHR}_{result} = \begin{cases} \text{FHR}_{est.} & \text{if } |\text{FHR}_{est.} - \text{FHR}_{pred.}| \leq 0.35 \text{Hz} \\ \text{FHR}_{pred.} & \text{otherwise} \end{cases}$$

The resulting fetal heart rate is then stored in a historical buffer, which uses the last 30 sec of estimates to generate the next prediction model. In the case where the estimate is invalid for an extended period of time (i.e. 30 sec), we maintain the last FHR value rather than use $FHR_{pred.}$. This accommodates for situations when the FHR is hidden behind a maternal component (or harmonic) for a long duration. As such, once the fetal signal moves away from the offending maternal component, it will be picked up by the system as a valid fetal estimate and continue normally.

VI. IN VIVO EVALUATION

To evaluate the approach, we developed a TFO system prototype, and captured *in vivo* measurements on at-term pregnant sheep/hypoxic fetal lambs. We compared the accuracy of the proposed approach to identify the FHR against the true FHR and a naïve approach, which is shown in Figure 4(a). The naïve approach only utilizes the maternal noise reduction and fetal estimation blocks to identify the FHR. Since the fetal sensitivity is larger at far SD distances, the naïve approach only uses the channel located furthest from the light source to estimate the fetal signal.

A. Hypoxic Fetal Lamb Animal Model

At-term pregnant sheep (136 gestational days) were used in this experiment. After undergoing anesthesia, a balloon catheter was placed in the aorta of the pregnant sheep, above the blood-supply to the uterus, and inflated in a graded-fashion to induce varying levels of hypoxia to the *in utero* fetal lamb. The inflation was held at each grade for 10-minutes to allow adequate time for the changes to be translated to the fetus. An arterial blood line was placed in the fetal lamb, and routed externally from the pregnant ewe, where blood-pressure was measured and intermittent blood sampling was performed. The fetal HR, was generated from the fetal blood pressure waveforms, and calculated by the anesthesia monitoring system. The maternal heart rate was recorded via a conventional pulse oximeter, and the respiratory rate was

¹Since each blood-draw removes a non-negligible amount of blood from the fetus, only intermittent blood sampling was performed to reduce blood-loss.

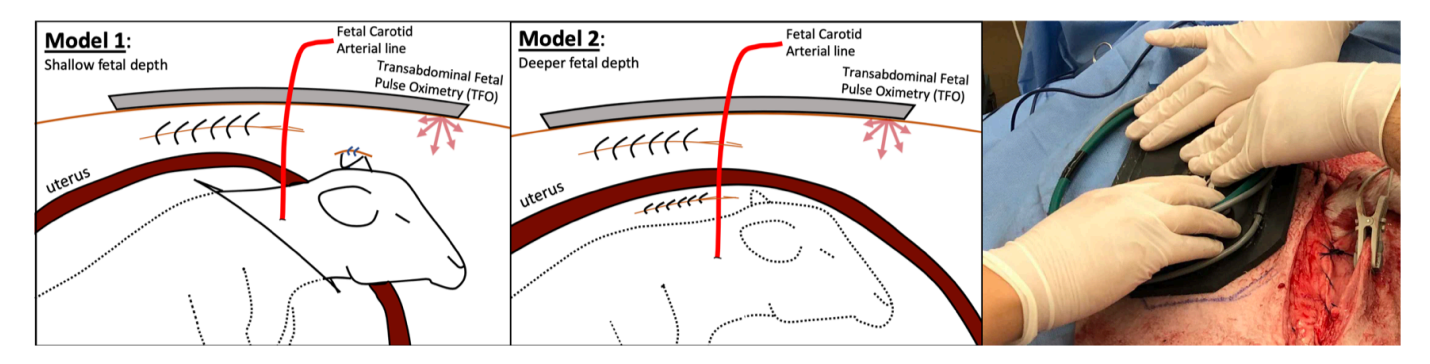


Fig. 5. Experimental setup of the Hypoxic Fetal Lamb Animal Models 1 and 2. Model 1 established a shallow fetal depth (1 cm), and Model 2 established a deep fetal depth (5 cm). An image of the optode being placed on the pregnant sheep during the experiment can be seen on the right.

captured through the anesthesia system which monitored the sheep's end-tidal CO2.

In this experiment, two fetal depths were evaluated which we label as Models 1 and 2. In Model 1, a shallow fetal depth of 1 cm was established by closing the uterus around the fetal neck, and suturing one ear of the fetus to the underside of the maternal abdominal wall. In Model 2, the fetus was fully-returned to the uterus, and previous incisions were closed with suture. In this case, the fetal depth was estimated to be about 5 cm. In both models, the amniotic fluid was replaced by warm saline. An illustration depicting the different animal models can be seen in Figure 5. All of the procedures were reviewed and approved by an Institutional Animal Care and Use Committee.

B. TFO System Prototype

To capture measurements on the pregnant ewes, we developed a TFO system prototype that consists of a multi-detector, optical body-sensor network, an optode control system, and custom software that controlled, captured, and displayed the light intensity signals in real-time, and is shown in Figure 6. Our optical body-sensor network consists of five detectors, which correspond to Si-photodiodes located on the optical probe (optode) with varying SD distances. The optode control system manages signal actuation and acquisition, and was designed and built on a custom printed-circuit board. Its submodules are briefly summarized here. The actuation/acquisition system uses lock-in detection to shift each wavelength-specific signal to a frequency with less flicker-noise. In addition, the acquisition pipeline also consists of several small-signal amplifiers, a high-resolution analog-to-digital converter, and a microcontroller which streams the data to custom software running on a laptop. The software, written in Java, follows a classic Model-View-Controller architecture and provides a GUI for user-control, real-time measurement feedback, and logs the information for post-processing.

C. Experimental Setup

Using our TFO system, measurements were taken on two pregnant ewes, one of which represented Model 1 (shallow fetal depth), and the other Model 2 (deep fetal depth). During the

experiments, the fetal parameters were logged intermittently to reduce the overall blood-loss to the fetus. The maternal parameters were also recorded and utilized in the maternal noise reduction scheme.

To evaluate the approach, we utilized five recordings (three from Model 1 and two from Model 2) of 10 minutes each. The naïve and proposed approaches were implemented in Matlab (MathWorks, Inc.), which were subsequently used to generate FHR estimates for each of the recordings (rounds). Their results were compared against the true FHR (captured at the fetal arterial line). Each 10 minute recording was analyzed using a 60 sec window, with a stride of 15 sec, where each window produces one FHR estimate. Since the *true* fetal parameters were only recorded intermittently, namely at 2.5 min, 5 min, and 10 min per recording, only three FHR estimates were compared for each round. To further highlight the efficacy of the approach, we also display the full FHR estimates next to the raw signal's spectrogram, which displays

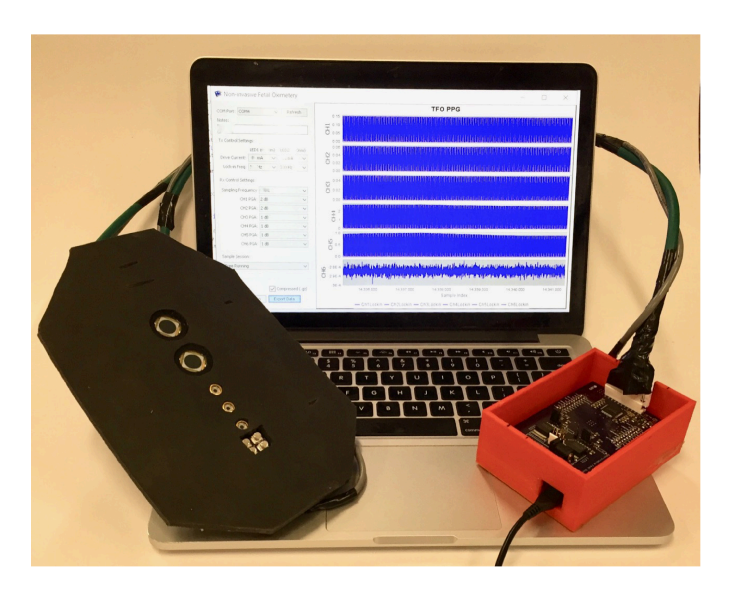


Fig. 6. Our Transabdominal Fetal Pulse Oximetry system used to capture measurements on the pregnant sheep. It consists of a multi-detector, optical body-sensor network (optode), an embedded optode control system, and custom software running on a laptop.

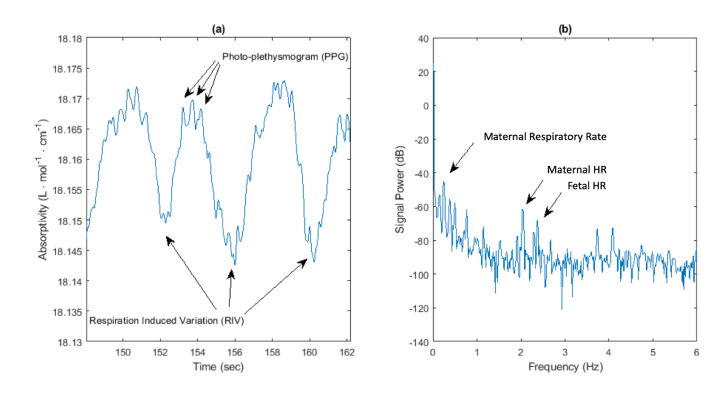


Fig. 7. Raw measurements captured on Channel 4 of Model 1, Round 2, annotated with the physiological signal sources. a) the raw time-series measurements and b) corresponding power spectral density.

the change in frequency content over time.

D. Results and Discussion

An example of the raw, time-domain signal captured at a channel and its power-spectral density can be seen in Figure 7. These raw signals were used to estimate the FHR using the naïve and proposed approaches and were compared with the true FHR measured via the fetal arterial line. Their results are shown in Table II. For clarity, we use the naming convention M1R3 to denote the 3rd Round of Model 1, and M2R1 to denote the 1st Round of Model 2. As shown, the root mean-squared error (RMSE) of the naïve method (0.581 Hz) is significantly worse than the proposed approach (0.159 Hz), suggesting that the contextually-aware approach is more accurate at identifying the fetal signal.

While intermittent recording of fetal parameters reduced overall fetal blood-loss, it limited the number of true FHR values to compare the approaches with. To highlight the efficacy of the approaches ability to track the fetal signal, we display the FHR estimates alongside the offending maternal respiration rate (MRR) and heart rates (MHR) from several rounds, next to a spectrogram of the raw measurements in Figure 8. The spectrogram displays the changes in frequency content over time, and provides a visual comparison to compare the FHR estimates with. For space reasons, the legend for the FHR estimates are shown in the M2R1 (zoomed) plot. The top row shows both maternal and fetal signal estimates, whereas the bottom row is scaled to highlight the changes in fetal signal estimates.

As shown in Figure 8, the FHR estimates from the proposed approach and naïve method work relatively well in most cases. However, when the fetal signal begins to approach a maternal harmonic, as seen in the bottom row of Figure 8, the naïve method fails drastically. In critical applications, such as fetal health monitoring, this can be dangerous as an important clinical-decision (such as performing an emergency C-section) may be made based on the instantaneous faulty data. For this reason, the *worst-case error* seen in a recording needs to be small. The worst-case error seen in each experiment is shown in Table II. For most of the experiments, the proposed

approach performed better than the naïve approach, whereas in others it performed equally-well. If evaluating the pregnant sheep from Models 1 and 2 as a whole, rather than by experiment, then the proposed approach performs drastically better than naïve method if looking at the worst-case error (Model 1: 1.33 Hz vs 0.18 Hz, Model 2: 1.17 Hz vs. 0.4 Hz, for naïve vs. proposed worst-case error, respectively).

To elaborate on the utility of the Maternal Noise Reduction and Data Fusion modules, we display a snapshot of the power spectral densities (PSD) in the M2R1 measurement recording in Figure 9. The PSD of the raw signals from each of the channels are shown in Figure 9(a), and shows that the signal contains a significant amount of maternal noise being generated by the mother's respiration and heart contractions, evident by the strong peaks at the MHR, MRR, and their harmonics. Without any context of the maternal physiology, identifying the fetal signal can be difficult. As such, by incorporating additional information about the mother's physiology, the maternal noise is reduced in each channel, of which the result can be seen in Figure 9(b). As can be seen, a strong peak in the PSD is present in several channels. The naïve method simply uses the channel with the largest SD distance (i.e. Ch5) and searches for the maximum power in the PSD between 2 to 5 Hz. In the proposed approach, however, data fusion is performed to create a spatially-aware signal that utilizes information from all of the detectors to improve the quality of the fetal signal before sending it to the Fetal Estimation module, the result of which can be seen in Figure 9(c). In this particular instance, both approaches (naïve and proposed) accurately identifies the true FHR.

VII. RELATED WORK

A large multi-center study evaluated the usage of transvaginal fetal pulse oximetry as a method to provide physicians with fetal oxygenation [26]. In this semi-invasive technique, an optical probe was inserted up the birth canal after the amniotic sac ruptures (i.e. water-breaks) to make contact with the fetus, where conventional reflectance-mode pulse oximetry was performed. The investigators found that the addition of fetal SpO2 helped with improving the confidence of fetal well-being in the face of indeterminate EFM traces. As such, *fully non-invasive* fetal oximetry can help provide a more convenient method of measuring fetal SpO2, through transcutaneous means. However, this introduces additional challenges, including patient variability and extracting the fetal signal.

To address these challenges in transabdominal fetal oximetry, several investigations have been performed that utilize Monte Carlo simulations to numerically characterize light propagation through the maternal and fetal tissue [19], [27], [28]. Others have used optical tissue phantoms to do this characterization or developed systems to mimic the pulsating tissue [29], [30]. Other investigations have looked at tackling the problem of fetal signal extraction, by investigating various signal processing techniques [31]–[33]. In one of the investigations [34], the authors used a comb filter to reduce maternal noise from simulated measurements, as well as through an

TABLE II
ESTIMATES OF THE HYPOXIC FETAL LAMB'S FETAL HEART RATE FROM NAÏVE AND PROPOSED APPROACHES

		FHR Estimate (Hz)			Error (Hz)		Worst-Case Error (Hz)	
Experiment	Time (Min)	Naive	Proposed Approach	True FHR (Hz)	Naive	Proposed Approach	Naive	Proposed Approac
Model 1, Round 1	2.5	2.367	2.367	2.43	0.063	0.063		
	5	3.733	2.283	2.467	1.266	0.184	1.266	0.184
	10	2.283	2.283	2.267	0.016	0.016		
Model 1, Round 2	2.5	3.733	2.3	2.4	1.333	0.1		0.1
	5	2.4	2.417	2.417	0.017	0	1.333	
	10	2.417	2.417	2.383	0.034	0.034		
Model 1, Round 3	2.5	2.217	2.217	2.183	0.034	0.034		0.034
	5	2.217	2.217	2.233	0.016	0.016	0.034	
	10	2.45	2.45	2.55	0.1	0.1		
Model 2, Round 1	2.5	3.2	3.2	3.233	0.033	0.033		0.083
	5	3.133	3.15	3.183	0.05	0.033	1.167	
	10	2.133	3.217	3.3	1.167	0.083		
Model 2, Round 2	2.5	3.55	3.55	3.167	0.383	0.383		0.4
	5	3.5	3.483	3.55	0.05	0.067	0.4	
	10	3.4	3.4	3	0.4	0.4		
oot Mean Squared Error (Hz)					0.581	0.159		

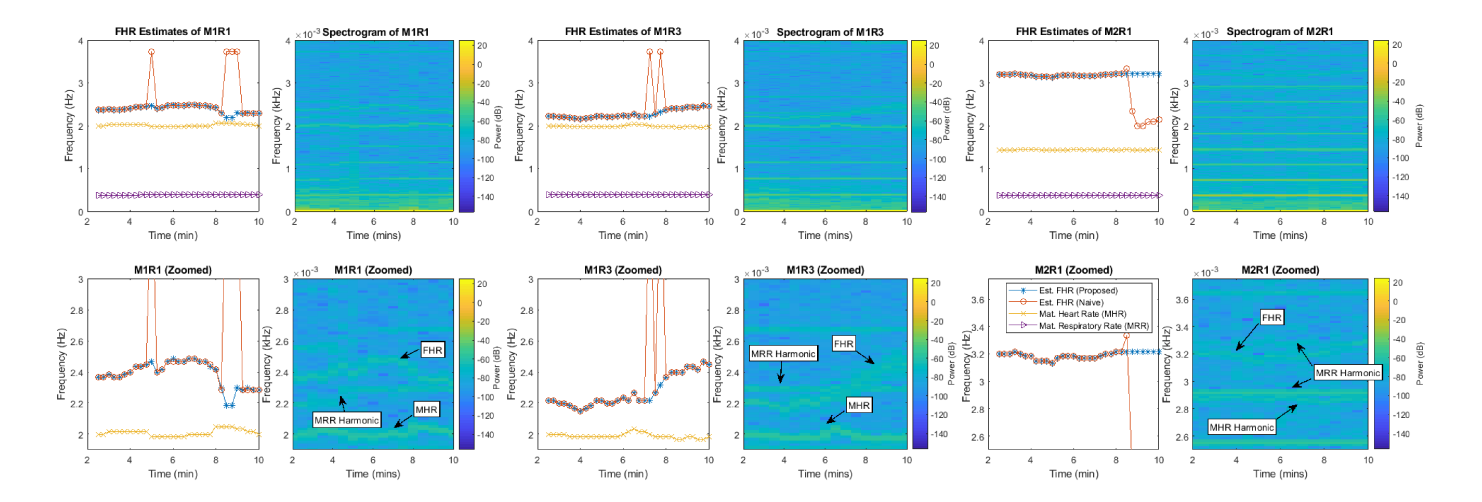


Fig. 8. Top row: Several traces of FHR estimates using the proposed and naïve approaches with the maternal components, next to the raw spectrogram. For visual clarity, the legend for all FHR estimates and maternal signals are found in the M2R1 (Zoomed) graph. Bottom row: the same traces zoomed in on the fetal signal, emphasizing the location of errors in reference to crossing a maternal component.

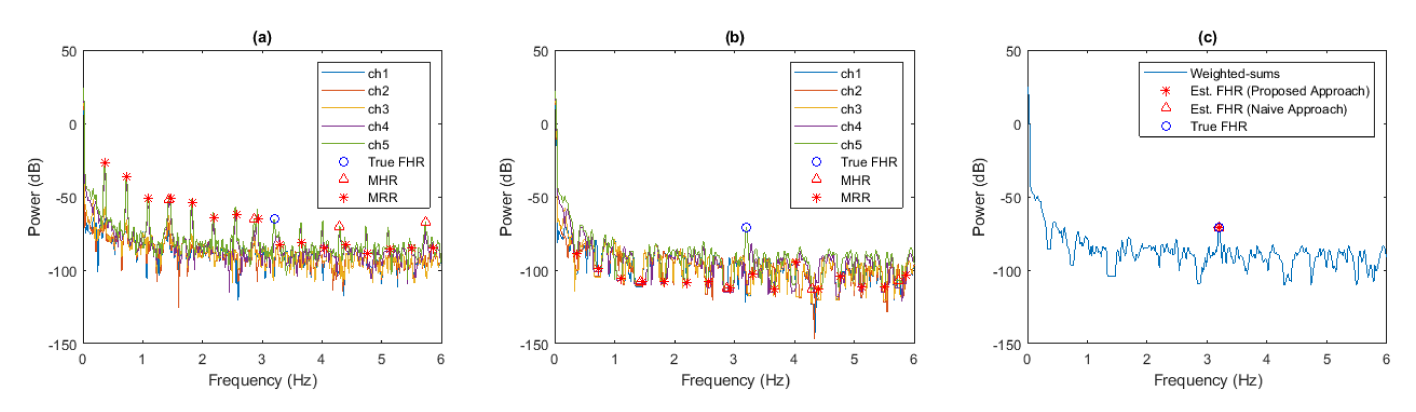


Fig. 9. A snapshot of the power spectral densities seen in the first round of Model 2 recordings using the proposed approach. a) raw signals from each channel, b) the signals exiting the Maternal Noise Reduction module, and c) the signal exiting the Data Fusion module, which combines all of the channels using a weighted-sums approach.

optical phantom, which performed well. Their technique represents a similar approach to the naïve method introduced in this paper. The authors in another study addresses the issue of patient variability by optimizing the optode design using a multi-objective optimization process [11].

VIII. CONCLUSION AND FUTURE WORK

In this paper, we presented an approach that estimates the fetal signal by incorporating additional physiological, spatial, and temporal context about the physical system. We evaluated the approach by capturing *in vivo* measurements on a pregnant sheep animal model, and compared the proposed approach with the true FHR. Currently, we are working on improving the system, and evaluating the system in an antepartum (prior to labor) scenario on pregnant human mothers.

REFERENCES

- K. B. Nelson, J. M. Dambrosia, T. Y. Ting, and J. K. Grether, "Uncertain value of electronic fetal monitoring in predicting cerebral palsy," *New England Journal of Medicine*, vol. 334, no. 10, pp. 613–619, 1996.
- [2] Z. Alfirevic, D. Devane, G. M. Gyte, and A. Cuthbert, "Continuous cardiotocography (ctg) as a form of electronic fetal monitoring (efm) for fetal assessment during labour," *Cochrane Database of Systematic Reviews*, no. 2, 2017.
- [3] T. F. Nielsen and K.-H. Hökegård, "Cesarean section and intraoperative surgical complications," *Acta Obstetricia et Gynecologica Scandinavica*, vol. 63, no. 2, pp. 103–108, 1984.
- [4] A. K. Hansen, K. Wisborg, N. Uldbjerg, and T. B. Henriksen, "Risk of respiratory morbidity in term infants delivered by elective caesarean section: cohort study," *BMJ*, vol. 336, no. 7635, pp. 85–87, 2008.
- [5] C. R. Cardwell, L. C. Stene, G. Joner, O. Cinek, J. Svensson, M. J. Goldacre, R. C. Parslow, P. Pozzilli, G. Brigis, D. Stoyanov, B. Urbonaité, S. Šipetić, E. Schober, C. Ionescu-Tirgoviste, G. Devoti, C. E. de Beaufort, K. Buschard, and C. C. Patterson, "Caesarean section is associated with an increased risk of childhood-onset type 1 diabetes mellitus: a meta-analysis of observational studies," *Diabetologia*, vol. 51, no. 5, pp. 726–735, May 2008.
- [6] J. A. Martin, B. E. Hamilton, M. J. Osterman, A. K. Driscoll, and P. Drake, "Births: Final data for 2017," *National Vital Statistics Reports*, 2018.
- [7] World Health Organization, "Appropriate technology for birth," The Lancet, vol. 326, no. 8452, pp. 436 – 437, 1985.
- [8] G. Molina, T. G. Weiser, S. R. Lipsitz, and et al, "Relationship between cesarean delivery rate and maternal and neonatal mortality," *JAMA*, vol. 314, no. 21, pp. 2263–2270, 12 2015.
- [9] L. Sabiani, R. L. Du, A. Loundou, C. d'Ercole, F. Bretelle, L. Boubli, and X. Carcopino, "Intra- and interobserver agreement among obstetric experts in court regarding the review of abnormal fetal heart rate tracings and obstetrical management," *American Journal of Obstetrics and Gynecology*, 2015.
- [10] E. L. Barber, L. S. Lundsberg, K. Belanger, C. M. Pettker, E. F. Funai, and J. L. Illuzzi, "Indications contributing to the increasing cesarean delivery rate," *Obstetrics and Gynecology*, vol. 118, no. 1, pp. 29–38, July 2011.
- [11] D. D. Fong, V. J. Srinivasan, K. Vali, and S. Ghiasi, "Optode design space exploration for clinically-robust non-invasive fetal oximetry," ACM Transactions on Embedded Computing Systems, vol. 18, no. 5s, 2019.
- [12] S. Pildner von Steinburg, A.-L. Boulesteix, C. Lederer, S. Grunow, S. Schiermeier, W. Hatzmann, K.-T. M. Schneider, and M. Daumer, "What is the "normal" fetal heart rate?" *PeerJ*, vol. 1, pp. e82–e82, 06 2013
- [13] J. G. Webster, Design of Pulse Oximeters. Institute of Physics Publishing, 1997.
- [14] L. Nilsson, A. Johansson, and S. Kalman, "Macrocirculation is not the sole determinant of respiratory induced variations in the reflection mode photoplethysmographic signal," *Physiological Measurement*, vol. 24, no. 4, 2003.

- [15] S. P. Linder, S. Wendelken, J. Clayman, and P. R. Steiner, "Noninvasive detection of the hemodynamic stress of exercise using the photoplethysmogram," *Journal of Clinical Monitoring and Computing*, 2008.
- [16] W. Karlen, S. Raman, J. M. Ansermino, and G. A. Dumont, "Multiparameter respiratory rate estimation from the photoplethysmogram," *IEEE Trans. Biomed. Engineering*, 2013.
- [17] P. L. Carson, J. M. Rubin, and E. H. Chiang, "Fetal depth and ultrasound path lengths through overlying tissues," *Ultrasound in Medicine and Biology*, vol. 15, no. 7, pp. 629–639, 1989.
- [18] C. R. Simpson, M. Kohl, M. Essenpreis, and M. Cope, "Near-infrared optical properties of ex vivo human skin and subcutaneous tissues measured using the monte carlo inversion technique," *Physics in Medicine and Biology*, vol. 43, no. 9, p. 2465, 1998.
- [19] D. Fong, A. Knoesen, and S. Ghiasi, "Transabdominal fetal pulse oximetry: The case of fetal signal optimization," in 2017 IEEE 19th International Conference on e-Health Networking, Applications and Services (Healthcom), Oct 2017, pp. 1–6.
- [20] P. M. Ripley, J. G. Laufer, A. D. Gordon, R. J. Connell, and S. G. Bown, "Near-infrared optical properties of ex vivo human uterus determined by the monte carlo inversion technique," *Physics in Medicine and Biology*, vol. 44, no. 10, p. 2451, 1999.
- [21] A. B. Modena and S. Fieni, "Amniotic fluid dynamics." Acta Biomed, vol. 75 Suppl 1, pp. 11–13, 2004.
- [22] S. Ijichi, T. Kusaka, K. Isobe, K. Okubo, K. Kawada, M. Namba, H. Okada, T. Nishida, T. Imai, and S. Itoh, "Developmental changes of optical properties in neonates determined by near-infrared time-resolved spectroscopy," *Pediatr Res*, vol. 58, no. 3, pp. 568–573, 09 2005.
- [23] W. G. Zijlstra, A. Buursma, and W. P. Meeuwsen-van der Roest, "Absorption spectra of human fetal and adult oxyhemoglobin, deoxyhemoglobin, carboxyhemoglobin, and methemoglobin." *Clin Chem*, vol. 37, no. 9, pp. 1633–1638, Sep 1991.
- [24] Q. Fang and D. A. Boas, "Monte carlo simulation of photon migration in 3d turbid media accelerated by graphics processing units," *Opt. Express*, vol. 17, no. 22, pp. 20178–20190, Oct 2009.
- [25] Wojakowski, Izbizky, Carcano, Aiello, Marantz, and Otano, "Fetal doppler mechanical pr interval: correlation with fetal heart rate, gestational age and fetal sex," *Ultrasound Obstetrics and Gynecology*, 2009.
- [26] T. J. Garite, G. A. Dildy, H. McNamara, M. P. Nageotte, F. H. Boehm, E. H. Dellinger, R. A. Knuppel, R. P. Porreco, H. S. Miller, S. Sunderji, M. W. Varner, and D. B. Swedlow, "A multicenter controlled trial of fetal pulse oximetry in the intrapartum management of nonreassuring fetal heart rate patterns," *American Journal of Obstetrics and Gynecology*, vol. 183, no. 5, pp. 1049–1058, 11 2000.
- [27] A. Zourabian, A. Siegel, B. Chance, N. Ramanujam, M. Rode, and D. A. Boas, "Trans-abdominal monitoring of fetal arterial blood oxygenation using pulse oximetry," *Journal of Biomedical Optics*, vol. 5, no. 4, pp. 391–405, 2000.
- [28] S. Ley, D. Laqua, and P. Husar, Simulation of Photon Propagation in Multi-layered Tissue for Non-invasive Fetal Pulse Oximetry. Cham: Springer International Publishing, 2014, pp. 356–359.
- [29] S. Ley, M. Stadthalter, D. Link, D. Laqua, and P. Husar, "Phantom materials mimicking the optical properties in the near infrared range for non-invasive fetal pulse oximetry," in 2014 36th Annual International Conference of the IEEE Engineering in Medicine and Biology Society, Aug 2014, pp. 1432–1435.
- [30] G. Vishnoi, A. H. Hielscher, N. Ramanujam, and B. Chance, "Photon migration through fetal head in utero using continuous wave, nearinfrared spectroscopy: development and evaluation of experimental and numerical models," *Journal of Biomedical Optics*, vol. 5, no. 2, pp. 163–172, 2000.
- [31] D. D. Fong, A. Knoesen, M. Motamedi, T. O'Neill, and S. Ghiasi, "Recovering the fetal signal in transabdominal fetal pulse oximetry," *Smart Health*, vol. 9-10, pp. 23 – 36, 2018.
- [32] E. Zahedi and G. K. Beng, "Applicability of adaptive noise cancellation to fetal heart rate detection using photoplethysmography," *Computers in Biology and Medicine*, vol. 38, no. 1, pp. 31–41, 1 2008.
- [33] M. Böttrich and P. Husar, "Extraction of the fetal pulse curve for transabdominal pulse oximetry using adaptive and comb filters," in 2019 41st Annual International Conference of the IEEE Engineering in Medicine and Biology Society (EMBC), July 2019, pp. 15–18.
- [34] M. Böttrich and P. husar, "Signal separation for transabdominal noninvasive fetal pulse oximetry using comb filters," in 2018 40th Annual International Conference of the IEEE Engineering in Medicine and Biology Society (EMBC), July 2018, pp. 5870–5873.